Results in Engineering 5 (2020) 100073

Contents lists available at ScienceDirect

Results in Engineering

journal homepage: www.editorialmanager.com/rineng/Default.aspx

Thermal and mechanical stresses in bayonet tubes of solar central receivers working with molten salt and liquid sodium

Rafael Pérez-Álvarez *, Antonio Acosta-Iborra, Domingo Santana

Department of Thermal and Fluids Engineering, Carlos III University of Madrid, Avda. de La Universidad 30, 28911, Leganés, Madrid, Spain

ARTICLE INFO

Keywords:
Solar power tower
Solar receiver
Bayonet tube
Thermal stresses
Molten salt
Liquid sodium
Non-uniform heat flux

ABSTRACT

One of the most promising technologies for solar thermal power are solar power towers (SPTs), in which direct solar radiation is redirected by heliostats to a receiver located on top of a tower. The technology used by SPT allows obtaining high thermal efficiencies as well as a high number of hours of operation thanks to thermal storage. However, the high thermal gradients to which the receiver is subjected, in addition to the corrosion of the molten solar salt, can cause the rupture of the receiver and this limits the maximum irradiation the receiver can withstand. To overcome this problem there are different strategies, such as the use of working fluids that are less corrosive than molten salts or the development of new designs of the receiver to avoid overheating of the pipes.

In this work we analyze the thermal and structural behavior of a new design of SPT receiver in which bayonet tubes are used instead of simple tubes. A bayonet tube consists of a tube inside another one. In the bayonet tube the working fluid first circulates through the inner tube and then through the annular section between the tubes. An eccentric bayonet tube, created by displacing the inner tube with regards the outer tube, reduces the overheating of the fluid and the outer tube wall as will be shown later. Besides, this work also assesses the effect of using either molten salt or liquid sodium as a working fluid on the thermal and structural behavior of the absorber tube. Since the extreme thermal conditions of central receivers preclude a detailed experimental analysis, the analyses of the present work are performed through multi-physics (CFD – FEM) simulations of the working fluid flow in the annular section and the stresses in the outer wall of the bayonet tube, which are the most critical elements of the receiver. In particular, to perform the hydrodynamic and thermal analysis of the fluid section and the outer wall of the tube, the RANS equations of the fluid together with the turbulent RSM model and the head diffusion equation of the wall were solved using ANSYS Fluent v18 CFD code. Boundary conditions of temperature and non-uniform irradiation were selected to represent typical operative conditions of receivers. Subsequently, using the temperature profiles obtained from the CFD simulations for each working fluid, ANSYS Workbench v18 was employed to obtain the thermal and mechanical stresses in the outer tube as a function of its different constraints, including the attachment of the tube.

The results obtained with the CFD – FEM simulations show that, regardless of the working fluid, the eccentricity of the bayonet tube decreases local peaks of temperature in the flow and temperature gradients in the outer tube wall, which leads to a reduction of the wall stresses of the SPT receiver. Furthermore, thanks to its high conductivity, liquid sodium is able to yield lower temperature gradients and stresses in the wall, independently of the kind of tube, compared to molten salt.

Introduction

The production of electricity using solar energy is experiencing an unprecedented increase due to the growing social awareness of the environment and the rising cost of fossil fuels. Among current applications of solar energy to produce electricity, Solar Power Tower plants (SPTs) stand out, comprising 71.43% of the total concentrating solar power (CSP) projects under development [1], because they have a higher thermal efficiency, around 78% [2], and can work during more hours thanks to thermal storage. In Fig. 1 (a) a scheme of SPT with a heliostast field, a thermal storage system and receiver can be observed. However, SPTs are far from their full potential as a result of the operation problems of these plants. One of the main problems resides in the rupture of the receiver tubes. As show in Ref. [3], the high temperature gradients lead to high thermal stresses in the tube. Both the temperature gradients and

* Corresponding author.
E-mail address: rafperez@ing.uc3m.es (R. Pérez-Álvarez).

https://doi.org/10.1016/j.rineng.2019.100073
Received 15 September 2019; Received in revised form 14 November 2019; Accepted 20 November 2019

Nomenclature

$\overline{U}$	Overall heat transfer coefficient of working fluid at bayonet inner tube
$\overline{T}$	Average working fluid temperature of bayonet inner tube
σ_θ	Circumferential normal stress component
σ_r	Radial normal stress component
σ_{VM}	Von Mises stress
σ_z	Axial normal stress component
τ_{xy}	XY shear stress component
τ_{xz}	XZ shear stress component
τ_{yz}	YZ shear stress component
θ	Angular position referred to the axis of the outer tube
$\theta^{'}$	Angular position referred to the axis of the internal tube
ξ	Eccentricity
D_e	Outer diameter of outside tube
d_e	Outer diameter of internal tube
D_i	Inner diameter of outside tube
e	Distance between the centers of the outside and internal tubes
k_{tube}	Thermal conductivity of tube walls
L	Length of the tube
Pr_i	Prandtl number evaluated at the inlet conditions
q''	Local heat flux
q''_{max}	Maximum value of heat flux
q''_{rerad}	Reradiant component of heat flux
R	Radial position referred to the axis of the outside tube
R''_f	working fluid fouling resistance
$R^{'}$	Radial position refer to axis of inner tube
Re_i	Reynolds number evaluated at the inlet conditions
T_E	Outer surface temperature of the outside tube
T_{inlet}	Temperature of working fluid at tube inlet
T_i	Temperature of working fluid at annular inlet
T_o	Temperature of working fluid at outlet
v_i	working fluid velocity at the inlet conditions
z	Axial position, height

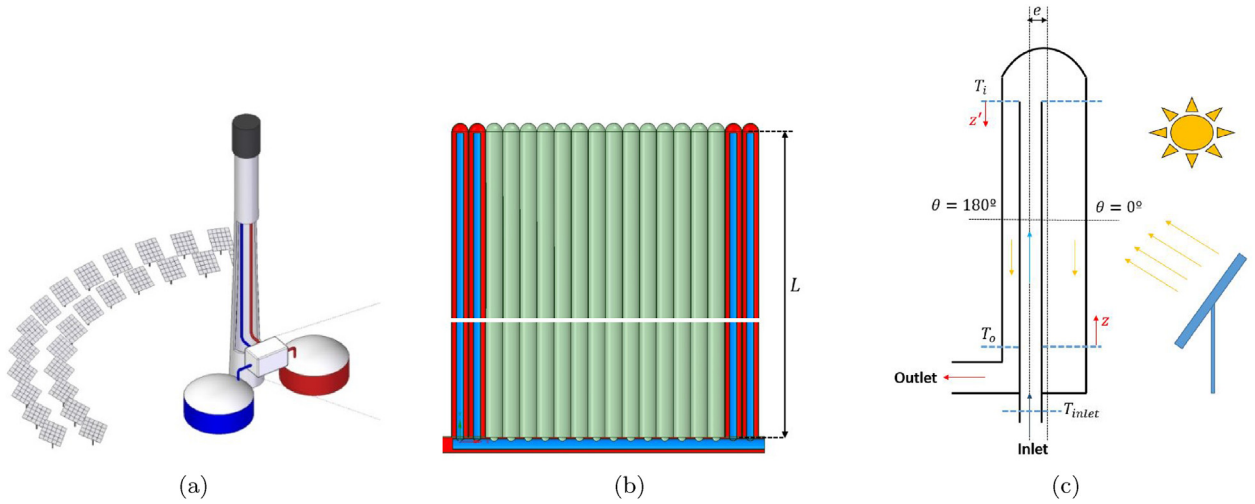

Fig. 1. (a) Basic configuration of a Solar Power Tower plant with the solar receiver (in black color) on top of a tower and with storage of high temperature (red) and low temperature (blue) working fluids (b) Example of a panel with bayonet tubes, (c) Schematic representation of a bayonet tube.

the thermal stresses are the principal causes of the substantial reduction of the useful-life [4]. There are different options to solve these problems, such as the substitution of the working fluid for a less corrosive one to avoid the corrosion of the working fluid, or the design of new receivers that reduce the overheating of the tube walls. There are previous works in the specialized literature about this topic. For example, in Ref. [5] a transient CFD comparison is made between molten salts and liquid metals. In Ref. [6], the distribution of temperatures and the heat flux are obtained in tubular sodium receptors. In Ref. [2] there is an analysis with simplified models of a solar receiver working with a molten salt as a working fluid. In this work two different types of solar receivers are studied: a conventional receiver consisting of simple tubes and a new concept of receiver, proposed in Ref. [7], consisting of bayonet tubes, Fig. 1(b). As schematized in Fig. 1(c), the bayonet tube is composed of one tube inside another. The working fluid flows first through the circular section of the inner tube and then back through the annular section formed between the inner and outer tubes. The heat absorbed by the outer tube, coming from the solar irradiation concentrated by the heliostats field, increases the temperature of the fluid flow in the annular section. A fraction of this heat is exchanged through the inner tube wall to the flow in the circular section, which is cooler, thus avoiding excessive overheating of the fluid in the annular section. When the axis of the inner tube is displaced from the center of the outer tube opposite to the angular direction where the solar radiation is maximum, $\theta = 0^o$, an asymmetry is created. This asymmetry affects the flow characteristics and can be used to increase the heat transfer coefficient in the angular direction of $\theta = 0^o$, Fig. 1(c). This configuration, which is called eccentric bayonet tube, opens the possibility of decreasing the surface temperature while reducing the pressure drop compared to simple tubes. The geometrical eccentricity can be defined as follows:

$$\xi = \frac{e}{D_i - d_e} \tag{1}$$

Where e is the distance between the centers of the inner and outer tubes, d_e is the outer diameter of the inner tube and D_i is the inner diameter of the outer tube. The effect of the eccentricity has been previously studied throught numerical simulation for molten salt [8] and for liquid sodium and sCO2 in Ref. [9]. In Ref. [10] an analytical model was developed to characterize the heat transfer in eccentric annular tube for a turbulent flow. However, in order to optimize the design of these receivers, it is necessary to study their structural behavior. The aim of the present work is to characterize, for a conventional tube receiver and a

bayonet tube receiver, the effects of the working fluid (molten salt or liquid sodium) and the type of mechanical attachment of the tubes on the thermal stresses of the tubes.

Numerical simulation

In order to obtain the structural stresses of the studied receivers, it is firstly necessary to characterize their thermal and hydrodynamic behaviors. In particular, a series of fluid dynamics simulations (CFD) are performed in this work to obtain the distributions of pressure and temperature created by each working fluid on the tube walls. Subsequently, these distributions are introduced as boundary conditions in the structural simulation of the tubes. The next sections present the main characteristics of these CFD and structural simulations.

CFD numerical simulation

For the simple tube, the complete geometry, i.e. fluid and solid domains, has been analyzed, Fig. 2 (a). On the CFD simulation of the bayonet tube, only the fluid in the annular zone and the outer tube have been analyzed, Fig. 2 (b), (c) because they are exposed to a high heat flux and they are the most complex and determinant elements for the characterization of a bayonet tube receiver. To create the geometry and the mesh of the fluid and solid fields, the commercial code ANSYS Workbench v18 has been used in this work.

The dimensions of the tubes are 2.11 *cm* for the outer diameter of the inner tube (d_e) and 4.46 *cm* for the outer diameter of the outer tube (D_e). The tube thickness is 1.2 *mm*. The both the circular section of the simple tube and the annular section of the bayonet tube are analyzed for a length of 10 *m*, similar to the dimensions used in Ref. [11]. A fundamental aspect to keep in mind is that the mesh for the fluid domain must be thin enough to capture adequately the elevated thermal gradient in the vicinity the outer walls. To verify the independence of the results with the CFD mesh a grid sensitivity study was performed. In this analysis local temperature at $\theta = 0^o$ and bulk temperature evaluated on a height of $z = 5m$ were studied for 4 meshes with different cells concentration in the radial direction. The number of cells for these meshes were: 3.56126×10^5, 7.12252×10^5, 1.360957×10^6 and 3.56475×10^6. The variation of bulk temperature and local temperature at $\theta = 0^o$ between the largest mesh (3.56475×10^6 cells) and the mesh with 1.360957×10^6 cells were 0.37% and 3.54% respectively. The compromise solution between precision and computational cost was obtained with the mesh of $1,360,957$, which was selected to calculate the results of this work. The CFD simulations of the velocity and temperature of the working fluids in the annular section of the bayonet tube (in concentric and eccentric configurations) and in the circular section of the single tube, were carried out with the commercial code ANSYS Fluent v18, [12]. The RANS equations of mass, momentum and energy were solved in three dimensions. In addition, the seven equations of the Reynolds Stress Model (RSM) were chosen to properly capture the anisotropy of the turbulence existing in the annular section [13]. All the equations were solved in a stationary state and second order of precision in the convective terms. The properties used in the simulation for the molten solar salt (60% $NaNO_3$ - 40% KNO_3), the liquid sodium and the tube material, Incoloy 800H alloy, are temperature dependent and have been taken from Refs. [14–16] respectively. The boundary conditions used in the simulations were obtained from Ref. [7] for the fourth-north panel, which is one of the panels subjected to the most extreme conditions in a receiver [17]. At the outlet of the tube, for the simple and the bayonet tubes, the pressure-outlet condition was imposed. Walls were considered as non-slip surfaces. According to a simplified model, not shown here for simplicity, the temperature of the working fluid on the inner tube of the bayonet tube does not present a high variation. Thus, as a first approximation to the problem, it was not necessary to simulate the flow in the circular section of the inner tube. Instead of the flow in the inner tube of the bayonet tube, an average flow temperature in the inner tube has been used, $\overline{T}$, together with a global heat transfer coefficient, $\overline{U}$, to couple the flow in the annular section of the tube with the flow in the inner tube. This global coefficient of heat transfer, calculated at average temperature conditions, includes the convection resistance of the flow in the circular section of the inner tube, computed with the convective coefficient from the Dittus-Boelter correlation [18], the conduction resistance of inner tube (Incoloy 800H alloy with $k_{tube} = 16.3\ W/mK$) and fouling resistance of working fluid ($R_f^{''} = 8.85 \cdot 10^{-5}\ m^2K/W$). The lateral surfaces at the tube wall extremes have been defined as adiabatic surfaces. According to the simplified model [7], the incident heat flux into the outer tube is longitudinally constant but changes in angular direction. Thus, the flow of the absorbed heat is maximum in the area of the receiver that is facing to the field of heliostats ($\theta = 0^o$), while the rear zone of the tube, $|\theta| \geq 90^o$, absorbs a uniform heat flux coming from the reradiating

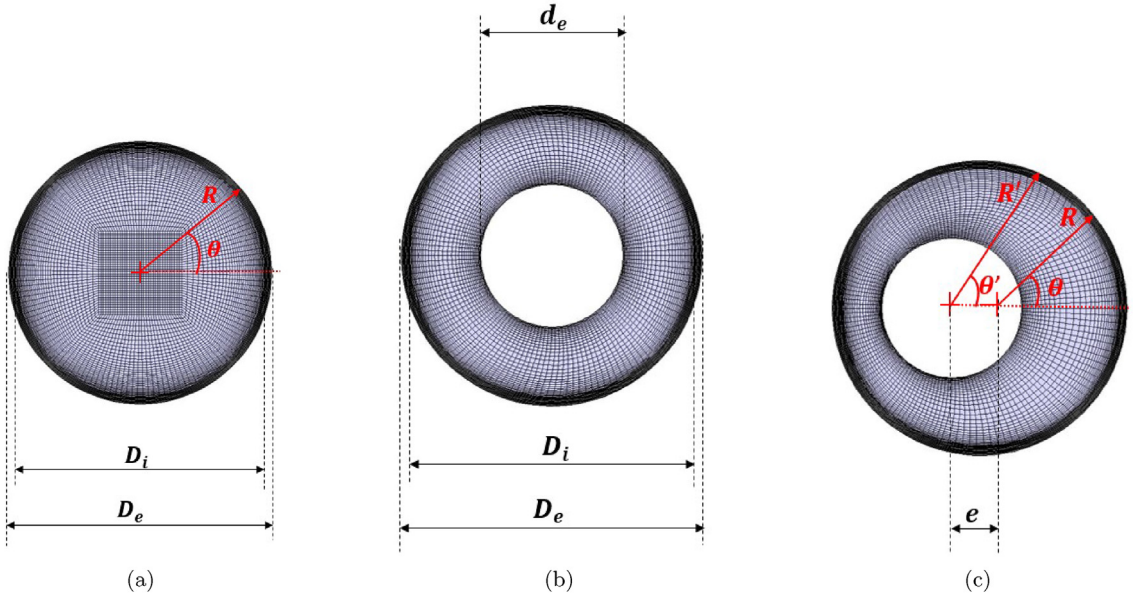

Fig. 2. Cross section of the mesh used for the CFD simulations and definition of nomenclature: (a) Simple tube, (b) Concentric bayonet tube ($\xi = 0.00$), (c) Eccentric bayonet tube ($\xi = 0.25$).

surface and the surrounding tubes. The complete distribution of the absorbed heat flux has been described in the simulation by a cosine function, which has been applied as a boundary condition at the outer surface of both the simple tube and the outer tube of the bayonet tube:

$$q^{''}(\theta) = \begin{cases} \left(q^{''}_{max} - q^{''}_{rerad}\right) \cdot cos(\theta) + q^{''}_{rerad} & if \quad |\theta| \leq 90^o \\ q^{''}_{rerad} & if \quad |\theta| > 90^o \end{cases} \tag{2}$$

where $q^{''}_{max} = 4.074 \cdot 10^5 W/m^2$ is the maximum irradiation heat flux per unit area and $q^{''}_{rerad}$ is the reradiating component, which has been set to 2.5% of $q^{''}_{max}$ similar to the value used in Refs. [8,9,11]. This reradiating component simulates the effect of the radiation that passes between the panel tubes and was obtained in Ref. [17] through numerical simulations.

In order to compare the simulations of single tube and bayonet tube receivers operating with different working fluids, the same temperature increase between the inlet and the outlet of the entire tube was imposed as well as the same incident heat flux and total heat absorbed. These conditions led to different mass flow rates for each CFD simulation. Table 1 summarizes the boundary conditions used in the simulation for the different working fluids and tubes analyzed.

Structural analysis

To characterize the mechanical behavior of bayonet and single tubes, a set of Finite Element Model (FEM) simulations were performed using the ANSYS Workbench v18 software. In the present work, the structural analysis is carried out for the simple tube and for the outer tube of the bayonet tube, which experience the largest thermal gradients and are affected by the attachments (clips) to the main structure. The inner tube of the bayonet tube does not suffer high thermal gradients compared to the outer tube. Therefore, the inner tube has not been analyzed in this work. As mentioned in the previous section, the material of the tubes is Incoloy 800H alloy [15], whose mechanical properties used in the structural analysis are temperature dependent.

A sensitivity analysis was performed into FEM mesh to verify the independence of the results with the mesh. In this analysis 4 meshes were studied having the following number of cells: 3.2125×10^4, 7.5698×10^4, 1.35459×10^5 and 4.55124×10^5. The difference of the Von Mises stress at $\theta = 0^o$ evaluated on a height of $z = 5m$ between largest mesh (4.55124×10^5 cells) and the selected mesh (1.35459×10^5 cells) is 4.37%. An example of cross section of compromise mesh used in the FEM analysis is shown in Fig. 3 (a).

The boundary conditions of the structural simulation are two folded: the mechanical constraints that are imposed to restrict the tube displacement, and the fields of pressure and temperature obtained previously in the CFD simulation. It is assumed that the displacements of the walls due to the pressure force and thermal expansion are relatively small, so that the working fluid is weakly affected by these displacements, which means that the temperature and pressure fields of a non-deformed tube can be directly imposed on the studied tube.

Typically, the tubes are attached to the receiver frame by means of clips, which are used to periodically guide the tubes along their length. The clips are joined through a weld to the back surface of the tubes, that is, at $\theta = 180^o$. In this work, the clip width has been defined as $2mm$, which is a representative value of this type of attachment. To analyze how the clips influence the mechanical stresses of the tube, two extreme configurations have been studied:

- First configuration, which is the most favorable situation because it has relatively how thermal stresses has low thermal stresses, since it does not have clips and the outer tube is encastred (i.e. zero relative displacement and rotation) at the outlet side connected with the outlet header, Fig. 3 (b). The other end of the tube is free to move since the bayonet tube has both headers on the same side, see Fig. 1 (c). In the present work, analogously to the bayonet tube, the simple tube without clips is encastred at the outlet but not at the inlet. In a real attachment, the simple tube is more restricted. For this reason, this simplification in the simple tube is intentionally done to place the simple tube in the most favorable stress conditions when it is compared with the bayonet tube.
- Second configuration, which is the most unfavorable situation since it has an infinite number of clips placed one after the other on the back surface of the tube, $\theta = 180^o$, as shown in Fig. 3 (c). The clips allow a displacement in the direction of the axis tube, while displacements in other directions are null. In this second configuration the outlet side of the tubes is also encastred as in the first configuration. The infinite number of clips represents an extreme case in which the lateral displacement at $\theta = 180^o$ is perfectly restricted. Although this ideal restriction is not real, it can be used in this study to analyze the basic contribution of lateral displacement restriction. It is envisioned that in a real configuration, with a finite number of clips, the resulting stresses would be contained between those obtained in the first and second configurations analyzed in this work.

Results

Wall temperature

In Fig. 4 (a, b) the angular variation of the surface temperature has been represented for the outer surface of the simple tube, the concentric bayonet tube ($\xi = 0.00$) and the eccentric bayonet tube ($\xi = 0.25$). This temperature is a critical variable, since it reflects how the working fluid is internally cooling the tube. The general behavior is that this temperature reaches a maximum in the side facing to heliostat field, $\theta = 0^o$, for all the cases studied, because in this direction the concentrated solar radiation is also maximum, Eq. (2).

The highest value of the temperature, for the conditions studied in this work, is reached at the exterior surface of a simple tube working with molten salt. If the working fluid is molten salt the bayonet tube with eccentricity leads to the smallest exterior temperature. However, if the working fluid is liquid sodium, the simple tube leads an exterior surface temperature that is smaller than the eccentric bayonet tube in all the angular directions excepting close to $\theta = 180^o$. This is because the high conductivity of the liquid sodium favors the uniformization of temperature in a simple tube more than in a bayonet tube, as the bayonet tube has the inner tube acting in this case as an obstacle to the direct conduction of heat from the front to the rear part of the tube. In general, as shown in Fig. 4 (a, b), eccentricity improves the cooling of the walls for bayonet tubes, so that the temperature at $\theta = 0^o$ decreases in all cases because the

Table 1
Boundary condition used in the CFD Simulation.

Tube	Fluid	Re_i	Pr_i	Inlet		Outlet	Inner Wall	
				T_i [K]	v_i [m/s]	T_o [K]	$\overline{U}[W/m^2K$	$\overline{T}[K]$
Bayonet	Molten Salt	$1.821 \cdot 10^4$	10.2	568.1	1.536	604.9	3481	565.6
	Liquid Sodium	$2.098 \cdot 10^5$	0.0057	573.9	3.816	602.9	52649	568.59
Simple	Molten Salt	$2.637 \cdot 10^4$	10.5	563.1	1.149	605.1	–	–
	Liquid Sodium	$3.076 \cdot 10^5$	0.0058	563.2	2.866	605.5	–	–

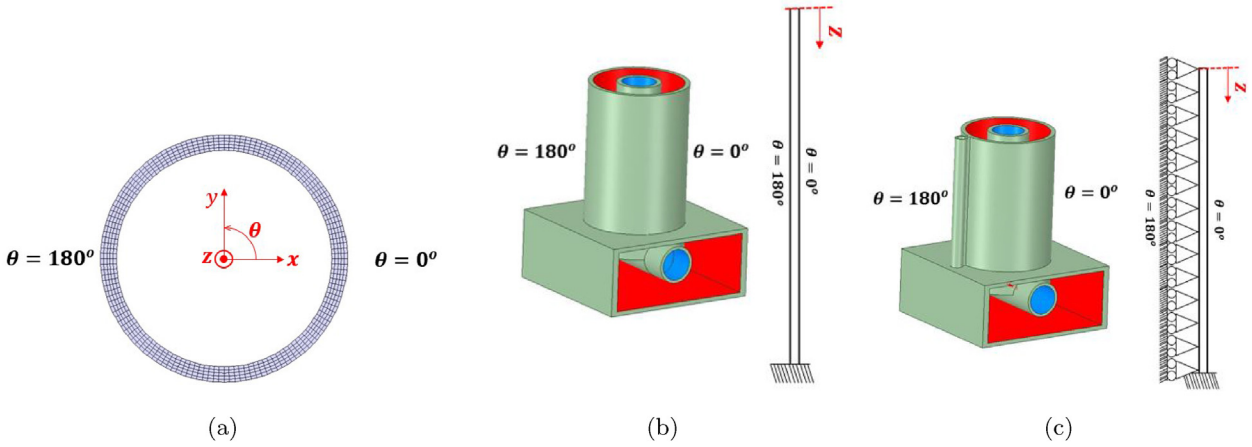

Fig. 3. (a) Cross section of the mesh used for the structural simulations. Mechanical restrictions used in the structural analysis: (b) Encastred tube without clips, (c) Encastred tube with an infinite array of clips.

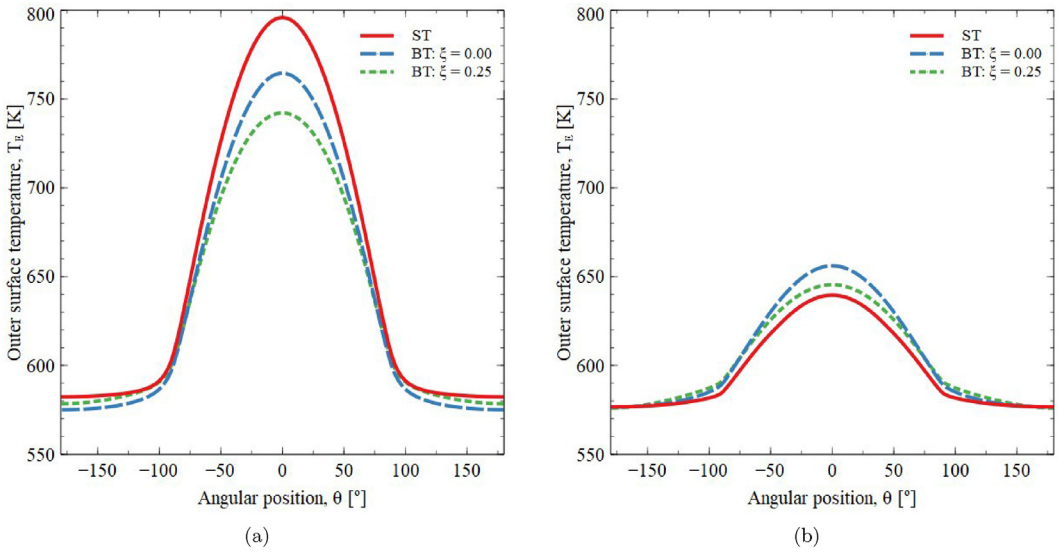

Fig. 4. Circumferential profile of the Von Mises stress for the configuration of encastred tube with clips. The simulation results correspond to the outer surface of the tube at $z = 5\ m$ from the tube inlet for (a) molten salt and (b) liquid sodium.

local velocity of the working fluid increases in a region near $\theta = 0^o$ when the eccentricity increases. This effect decreases the temperature of the outer wall for $|\theta| < 90^o$ because the fluid can absorb more heat from the walls. For $|\theta| > 90^o$ the wall temperature increases with the eccentricity due to the reduction of the axial velocity of the fluid in that region. This reduction of the temperature difference between the average and the front of the outer tube causes a decrease of the thermal stresses as shown in Ref. [3]. Regarding the change of working fluid, a considerable reduction in temperatures is observed when operating with liquid sodium, thanks to its high conductivity as mentioned before.

Regarding the axial distribution of the temperature at the exterior surface of the tubes, an approximately linear evolution of the temperature with height (axial coordinate, z) is obtained, as exemplified in Fig. 5 (a, b) for $\theta = 0^o$. In addition, this axial temperature profiles evidence a zone of thermal development for both the molten salt and the liquid sodium. The difference between the thermal development lengths of salt and sodium are explained in Ref. [19], and it is the reason of the temperature variation that appears when $z < 1\ m$.

Wall stresses

The distribution of the stress components in a cross section of the outer surface of the simple tube for the molten salt is shown in Fig. 6 (a, b), at a distance of $z = 5\ m$ from the inlet section. Only the outer surface results are showed, because they have the highest stresses. This figure helps to understand the impact of the thermal gradients of the tube wall, the attachment clips, and the internal pressure of the fluid, on the thermal stresses of the tubes. It can be seen that the most significant stress component is σ_z, which is the normal stress in the direction of the axis of the tube. The configuration without clips has three absolute maxima localized at $\theta = \pm 90^o$ and $\theta = 0^o$, where there are traction and compression zones. When the clips are introduced, the magnitude of the maxima located in $\theta = \pm 90^o$ is reduced, accentuating the stress component at $\theta = 0^o$. In the configuration without clips (see Fig. 6 (a)), the largest Von Mises stresses are located at $\theta = \pm 90^o$, due to traction stresses created in this area as a consequence of thermal expansion of the tube in the frontal region ($\theta = 0^o$). Besides, as a result of the different expansions of the rear and front sides of the tubes, the tubes are bent when they do not have clips. In the configuration with an infinite number of clips (Fig. 6 (b)), the tube can only move freely in axial direction, so that the expansion of the material cannot bent the tube because clips restrict the displacement. Therefore, in terms of normal stresses, the clips counteract the bending tendency of the tube, but this leads to a higher compressive stress in axial direction in the front of the tubes, which

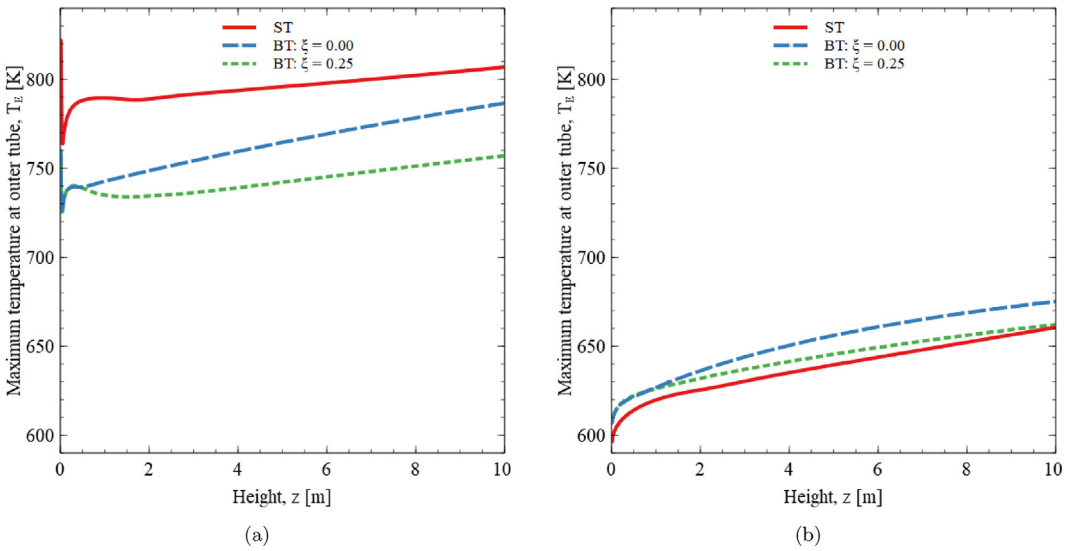

Fig. 5. Axial distribution of temperature at $\theta = 0^o$ for the exterior surface of both the simple tube and the outer tube of the bayonet tube. Simulation results for: (a) Molten salt and (b) Liquid sodium.

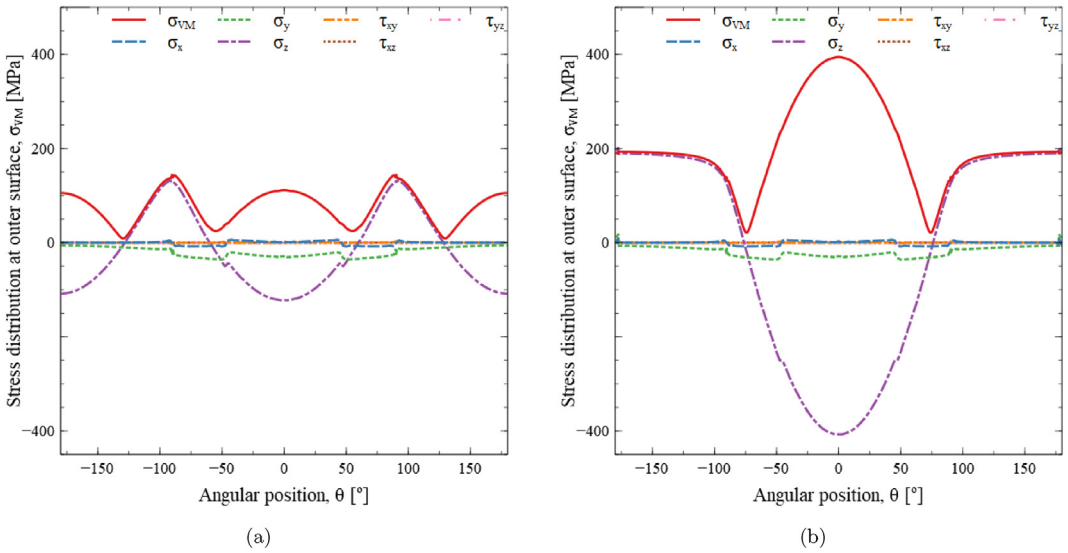

Fig. 6. Angular distribution of the axial (z), angular (θ), radial (r) and Von Mises (VM) stresses at the outer surface of the simple tube. Results are obtained with the simulation at a distance of $z = 5\ m$ from the inlet section of the simple tube for different attachment configurations: (a) without clips and (b) with clips.

presents the highest temperatures, and a higher traction stress in the rear side of the tubes.

The behavior of the thermal stresses described above occurs for both the simple tube and the bayonet tube. To analyze all the stress components in a single parameter, the equivalent Von Mises stress has been obtained from the simulation results.

Fig. 7 (a, b) contains the circumferential variation of the Von Mises stress at $z = 5\ m$ from the tube inlet, when it is operated with either molten salt or with liquid sodium in a configuration without clips. When molten solar salt is the working fluid, Fig. 7 (a), the simple and the bayonet tubes have a greater stress at $\theta = \pm 90^o$. The bayonet tube operating with solar salt and without clips can reduce the maximum stress in the tube, which appears at $\theta = \pm 90^o$, compared with the case of a simple tube. In contrast, for liquid sodium, the maximum stress is located at $\theta = 0^o$. As shown in Fig. 7 (b) the values of the Von Mises stress in the simple and the concentric bayonet tubes are similar when the working fluid is liquid sodium. However, regardless the working fluid is molten salt or liquid sodium, the eccentric bayonet tube is able to reduce the Von Mises stress compared to the simple tube.

Fig. 8 (a, b) shows the axial distribution of the maximum Von Mises stress. There is a zone of maximum stress in the section where the tube is encastred because the difference between the wall temperature at $\theta = 0^o$ and the average wall temperature is maximum and it is the principal cause of thermal stresses [3]. Moreover, any displacement of the material is restricted in the section $z = 0\ m$, but this is only an artificial singularity created by this perfect restriction. For $z > 0$, the Von Mises stress decreases gradually with z. The fact that the stress is not uniform along the length of the tube may be due to reduction of the temperature difference along the wall of the tube, which is the principal contributor to the thermal stresses. This explanation can be applied to the analysis with the configuration with infinite clips.

Fig. 9 and Fig. 10 show the Von Mises stress for the configuration of an encastred tube with an infinite number of clips. This case leads to the same general behavior as the case without clips. The circumferential profile of the Von Mises stress is not uniform, Fig. 9 (a, b), but now the values of the Von Mises stress are higher due to the restriction in the tube bending as discussed previously. The Von Mises stress increases with clips and it is between 2 and 3 times higher to that obtained without clips,

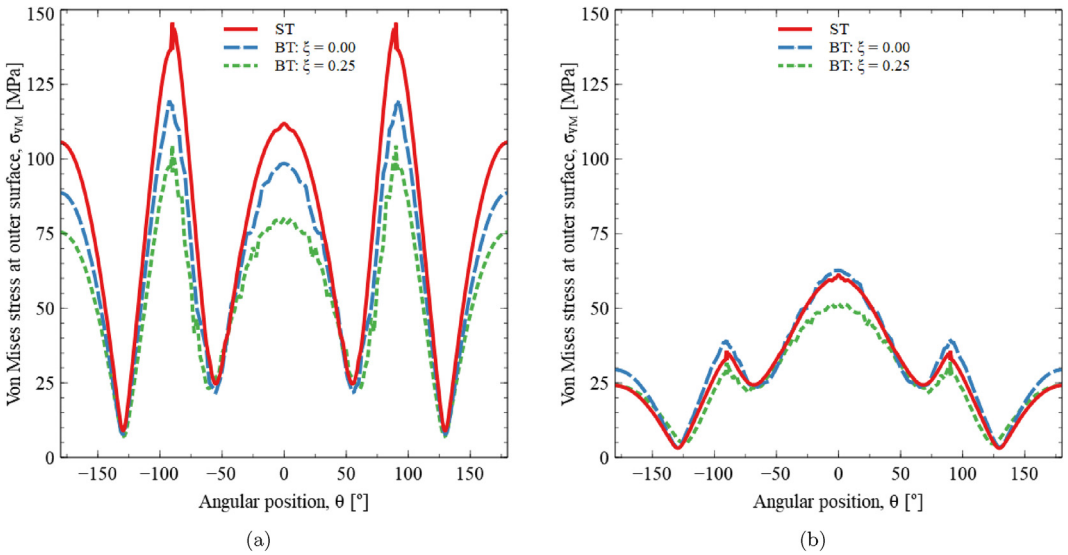

Fig. 7. Circumferential profiles of Von Mises stress for the configuration of encastred tube without clips. The simulation results correspond to the outer surface of the tube at $z = 5\ m$ from the tube inlet for (a) molten salt and (b) liquid sodium.

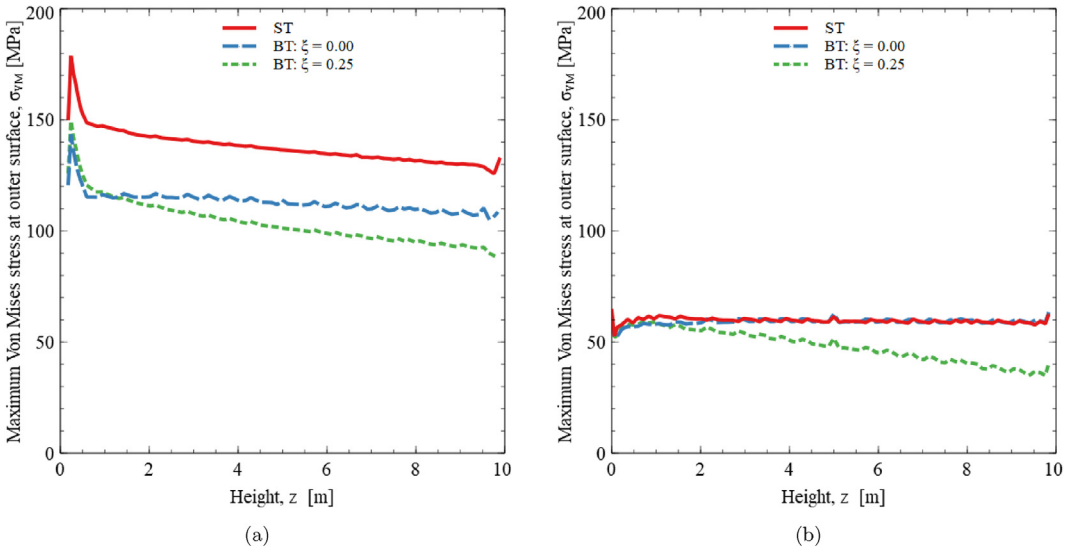

Fig. 8. Axial profile of Von Mises stress at the outer surface of the tube and $\theta = 90^o$. Simulation results for: (a) molten salt and (b) liquid sodium.

regardless of the working fluid. In a real configuration, this increase in stress is expected to be less acute because the clips are not perfectly rigid. Again, the configuration of the bayonet tube is capable of reducing the maximum stresses compared to a simple tube for the case of the molten salt, while for liquid sodium the opposite situation occurs; that is, the simple tube with liquid sodium is slightly more advantageous than the eccentric bayonet tube. In addition, comparing Figs. 7 and 9, it can be seen that the eccentricity reduces the Von Mises stresses at the front of the tube, $\theta = 0^o$ for the configuration of a bayonet tube. Reduction of the maximum temperature of the absorber tube and the maximum stresses leads to an increase of the receiver life [4].

Conclusions

The results for the CFD and the structural simulations of this work indicate that bayonet tubes, in both concentric and eccentric configurations, are advantageous over conventional tubes when they are operated with molten salt. Bayonet tubes can effectively reduce the temperature gradients and thermal stresses in the outer tube, regardless of whether the lateral movement of the tubes is restricted or not with clips. In particular, as the eccentricity of the bayonet tube increases the local velocity of the working fluid flow near the front surface of the outer wall, $|\theta| < 90^o$, the outer tube temperature in this region is also reduced. Therefore, according to the simulations, this reduction on temperature in the bayonet tube, leads to a decrease of the Von Mises thermal stress, compared to that of simple tube, when the working fluid is molten salt. For the tube without clips, the eccentricity helps to reduce the maximum stress of Von Mises, which appears in the outer tube at $\theta = \pm 90^o$. For the configuration with clips, an increase in the eccentricity of the bayonet tube allows a significant reduction of the Von Mises stress at the front of the tube, $\theta = 0^o$. When the working fluid is liquid sodium, due to its high thermal conductivity, the difference of temperature between the front and rear regions of the wall decreases due to a homogenization of the fluid temperature in a given cross section. This temperature homogenization caused by liquid sodium leads to a reduction of the Von Mises stress in both the simple tube and the outer tube of the bayonet tube. With the exception of the tube with clips operated with liquid sodium, the eccentric bayonet tube is able to reduce the thermal stress below that of a simple tube.

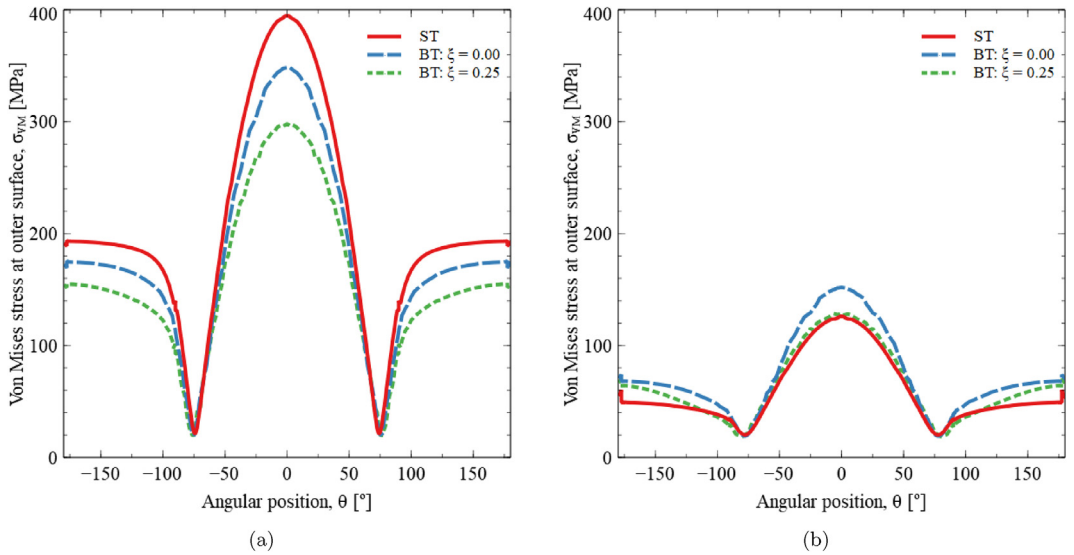

Fig. 9. Circumferential profile of the Von Mises stress for the configuration of encastred tube with clips. The simulation results correspond to the outer surface of the tube at $z = 5\ m$ from the tube inlet for (a) molten salt and (b) liquid sodium.

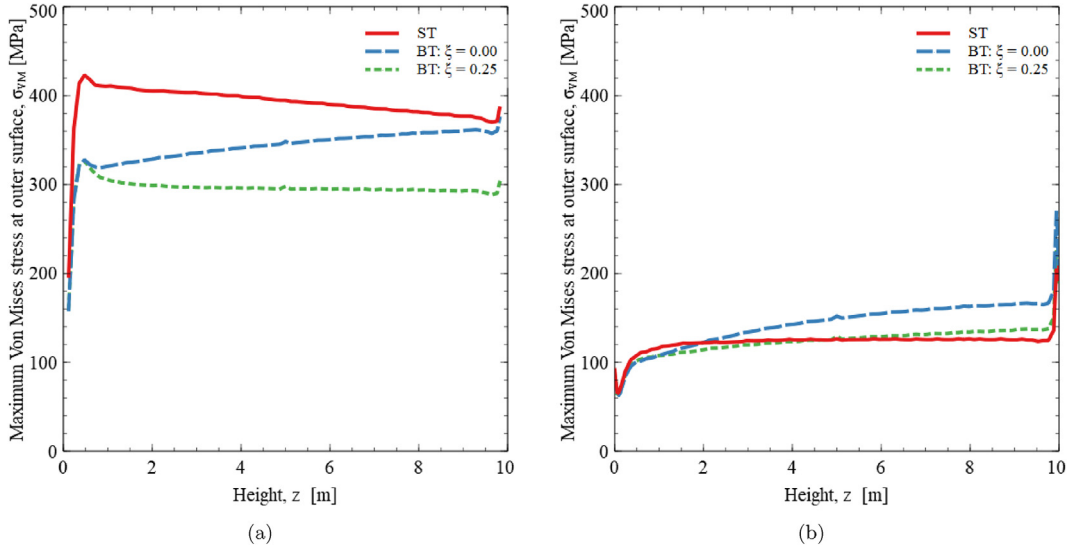

Fig. 10. Axial profile of the Von Mises stress at the outer surface of the tube and $\theta = 0^o$ for (a) molten salt and (b) liquid sodium.

Author contribution section

Rafael Pérez-Álvarez: Conceptualization, Methodology, Software, Formal analysis, Writing - Original Draft. Antonio Acosta-Iborra: Conceptualization, Validation, Writing - Review & Editing, Supervision. Domingo Santana: Conceptualization, Validation, Writing - Review & Editing, Supervision.

Declaration of competing interest

The authors declare that they have no known competing financial interests or personal relationships that could have appeared to influence the work reported in this paper.

Acknowledgements

The authors are grateful to acknowledge the financial support provided by Spanish Government for the project ENE2015-69486-R (MINECO/FEDER, UE), RTI2018-096664-B-C21 (MICINN, FEDER/UE) and the scholarship "Ayudas para contratos predoctorales para la formación de doctores" BES-2016-078455 awarded by the Ministerio de Economía, Industria y Competitividad.

References

[1] D.A. Baharoon, H.A. Rahman, W.Z. Wan Omar, S.O. Fadhl, Historical development of concentrating solar power technologies to generate clean electricity efficiently – a review, Renew. Sustain. Energy Rev. 41 (2015) 996–1027, https://doi.org/10.1016/j.rser.2014.09.008. ISSN 1364-0321.

[2] M.R. Rodríguez-Sánchez, A. Soria, J.A. Almendros-Ibáñez, A. Acosta-Iborra, D. Santana, Thermal design guidelines of solar power towers, Appl. Therm. Eng. 63 (2014) 428–438, https://doi.org/10.1016/j.applthermaleng.2013.11.014, 02.

[3] M.R. Rodríguez-Sánchez, C. Marugán-Cruz, A. Acosta-Iborra, D. Santana, Thermo-mechanical modelling of solar central receivers: effect of incident solar flux resolution, Sol. Energy 165 (2018) 43–54, https://doi.org/10.1016/j.solener.2018.03.005. ISSN 0038-092X.

[4] A. Mendelson, E. Roberts Jr., S.S. Manson, Optimization of time-temperature parameters for creep and stress rupture, with application to data from German cooperative long-time creep program, in: National Aeronautics and Space Administration Cleveland Oh Lewis Research Center, 1965. Technical report.

[5] A. Fritsch, R. Uhlig, L. Marocco, C. Frantz, R. Flesch, B. Hoffschmidt, A comparison between transient cfd and fem simulations of solar central receiver tubes using molten salt and liquid metals, Sol. Energy 155 (2017) 259–266, https://doi.org/10.1016/j.solener.2017.06.022. ISSN 0038-092X.

[6] W. Logie, C.A. Asselineau, J. Pye, J. Coventry, Temperature and heat flux distributions in sodium receiver tubes, in: Proceedings of the 2015 Asia-Pacific Solar Research Conference, 2015.
[7] M.R. Rodríguez-Sánchez, A. Sánchez-González, C. Marugán-Cruz, D. Santana, New designs of molten-salt tubular-receiver for solar power tower, ISSN 1876-6102, Energy Procedia 49 (2014) 504–513, https://doi.org/10.1016/j.egypro.2014.03.054. Proceedings of the SolarPACES 2013 International Conference.
[8] R. Pérez-Álvarez, M.R. Rodriguez-Sanchez, A. Acosta-Iborra, D. Santana, Effect of Eccentricity on the Hydrodynamics and Heat Transfer of Molten Salt in Bayonet Receivers for Solar Power Towers, vol. 2033, 2018, 080004, https://doi.org/10.1063/1.5067093, 11.
[9] R. Pérez-Álvarez, C. Marugan-Cruz, D. Santana, A. Acosta-Iborra, Comparison of the Heat Transfer Characteristics of Molten Salt, Liquid Sodium and Supercritical Co2 in Bayonet Tubes of Solar Tower Receivers, vol. 2126, 2019, 080005, https://doi.org/10.1063/1.5117600, 07.
[10] N. Nikitin, H. Wang, S. Chernyshenko, Turbulent flow and heat transfer in eccentric annulus, J. Fluid Mech. 638 (2009) 95–116, https://doi.org/10.1017/S002211200900812X.
[11] R. Pérez-Álvarez, Marta Laporte-Azcué, Antonio Acosta-Iborra, Domingo Santana, Effect of eccentricity on the thermal stresses in a bayonet tube for solar power tower receivers 2126 (2019b), 030041, https://doi.org/10.1063/1.5117553, 07.
[12] ANSYS Inc, Ansys 19 Fluent User Guide, Computer Methods in Applied Mechanics and Engineering, 2019. ISSN 5.
[13] E. Merzari, H. Ninokata, Anisotropic turbulence and coherent structures in eccentric annular channels, Flow, Turbul. Combust. 82 (1) (2009) 93–120, https://doi.org/10.1007/s10494-008-9170-2. Jan.
[14] A.B. Zavoico, Solar Power Tower Design Basis Document, Sandia National Labs, 2001, p. 7, https://doi.org/10.2172/786629.
[15] ASME Boiler, ASME Boiler and Pressure Vessel Code, Section II-Materials (Includes Addenda for 2011), American Society of Mechanical Engineers (ASME), 2010, 2011.
[16] V. Sobolev, Database of Thermophysical Properties of Liquid Metal Coolants for Gen-Iv, BLG-1069), 2011.
[17] M.R. Rodríguez-Sánchez, C. Marugan-Cruz, A. Acosta-Iborra, D. Santana, Comparison of simplified heat transfer models and cfd simulations for molten salt external receiver, Appl. Therm. Eng. 73 (1) (2014) 993–1005.
[18] L.M.K. Boelter, F.W. Dittus, Heat transfer in automobile radiators of the tubular type, Int. Commun. Heat Mass Transf. 12 (1) (1985) 3–22, https://doi.org/10.1016/0735-1933(85)90003-X.
[19] F.P. Incropera, A.S. Lavine, T.L. Bergman, D.P. DeWitt, Fundamentals of Heat and Mass Transfer, Wiley, 2007.